Myelin-reactive B cells exacerbate the severity of CD4$^+$ T cell-driven CNS autoimmunity in an IL-23-dependent manner.

Mohamed Reda Fazazi[1], Prenitha Mercy Ignatius Arokia Doss[1], Resel Pereira[2], Neva Fudge[3,4], Aryan Regmi[2,5], Irshad Akbar[1], Asmita Pradeep Yeola[1], Benoit Mailhot[1], Joanie Baillargeon[1], Philippe Grenier[6], Nicolas Bertrand[6,7], Steve Lacroix[1,8], Craig S. Moore[3,4], Olga L. Rojas[2,5], Manu Rangachari[1,8,9].

[1] axe Neurosciences, Centre de recherche du CHU de Québec – Université Laval, Pavillon CHUL, 2705 boul Laurier, Quebec City, QC, CANADA G1V 4G2; [2] Krembil Research Institute, University Health Network, Toronto ON CANADA M5T 0S8; [3] Division of BioMedical Sciences and [4] Department of Neurology, Faculty of Medicine, Memorial University of Newfoundland, St. John's NL, CANADA, A1B 3V6; [5] Department of Immunology, University of Toronto, Toronto ON, CANADA, M5S 1A1; [6] axe Endocrinologie et nephrologie, Centre de recherche du CHU de Québec – Université Laval, Pavillon CHUL, 2705 boul Laurier, Quebec City, QC, CANADA G1V 4G2; [7] Faculty of Pharmacy, Laval University, 1050 ave de la Médecine, Quebec City, CANADA; [8] Department of Molecular Medicine, Faculty of Medicine, Laval University, 1050 ave de la Médecine, Quebec City, CANADA; [9] Corresponding author.

Abstract

Multiple sclerosis (MS) is an autoimmune disorder of the central nervous system (CNS) that has traditionally been considered a T cell-mediated disease. However, accumulating evidence points to a crucial role for B cells in disease processes. IgH$^{[MOG]}$ mice possess a transgenic immunoglobulin heavy chain derived from a monoclonal antibody specific to myelin oligodendrocyte glycoprotein (MOG), a key target for autoimmune responses. Here, using the experimental autoimmune encephalomyelitis (EAE) model of MS, we investigated the susceptibility of IgH$^{[MOG]}$ mice to CD4^{+} T cell-driven disease that was induced by active immunization with MOG$_{[35-55]}$ autoantigen. We found that immunized IgH$^{[MOG]}$ mice rapidly developed severe EAE. While the frequency and absolute number of CNS-infiltrating B cells was similar between WT and IgH$^{[MOG]}$ mice, a greater frequency of class-switched and inflammatory cytokine-positive B cells were seen in the IgH$^{[MOG]}$ CNS. We observed an increased presence of class-switched and inflammatory cytokine-positive B cells in the IgH$^{[MOG]}$ CNS, as well as a greater frequency of IL-17- and GM-CSF-producing CD4^{+} T cells. Production of the Th17 maintenance factor IL-23 was increased from IgH$^{[MOG]}$ CNS-infiltrating B cells, and *in vivo* blockade of IL-23p19 strongly attenuated disease severity in IgH$^{[MOG]}$ mice. Strikingly, we observed an increased frequency of PD-1^{+}CXCR5^{-} T peripheral helper (Tph)-like cells in the CNS of IgH$^{[MOG]}$ mice and we also found that the meninges of immunized IgH$^{[MOG]}$ mice were characterized by an accumulation of tertiary lymphoid organs. Both Tph accumulation in the CNS, as well as meningeal inflammation, were again sharply reduced upon IL-23p19 blockade *in vivo*.

Intriguingly, the expression of *IL23a* transcript in the cerebrospinal fluid of MS-affected individuals was positively correlated with the frequency of B cells. Altogether, these data show that MOG-specific B cells contribute to severe $CD4^+$ T cell-driven EAE by promoting CNS accumulation of Th17 and Tph cells, as well as tertiary lymphoid organs in the CNS meninges, in an IL-23 dependent manner.

Keywords: experimental autoimmune encephalomyelitis, multiple sclerosis, B cell, $CD4^+$ T cell, myelin oligodendrocyte glycoprotein (MOG), IgH[MOG], 1C6, non-obese diabetic (NOD), Th17, IL-23, T-peripheral helper cells (Tph cells), tertiary lymphoid organ.

57 **Introduction**

58 Multiple sclerosis (MS) is a chronic autoimmune disease in which the adaptive
59 immune system launches an attack against central nervous system (CNS)
60 proteins, such as myelin. MS affects more than 2 million people worldwide [1].
61 Approximately 80% of patients present an initially relapsing-remitting (RR) disease
62 course for which there are now more than 10 disease-modifying therapies
63 available. However, 30-60% of these RR patients will eventually transition to a
64 chronically worsening secondary progressive (SP) phase, for which treatment
65 options are limited [2]. Pathophysiological mechanisms in progressive MS are thus
66 of intense current interest [3].

67 T cells, and $CD4^+$ T cells in particular, have historically been the most
68 intensively studied players in the immune pathogenesis of MS. However, it has
69 become increasingly clear that B cells additionally play important roles in MS
70 pathogenesis. Clonally expanded B cells are present in the cerebrospinal fluid
71 (CSF) and MS plaques[4-6], and the presence of meningeal follicles adjacent to
72 cortical lesions is associated with disease progression[7,8]. Further, antibodies
73 against myelin oligodendrocyte glycoprotein (MOG), a key component of myelin,
74 were found in active MS lesions [9]. Crucially, the B cell-targeting anti-CD20 drugs
75 rituximab[10], ocrelizumab[11] and ofatumumab[12] improve RRMS, and ocrelizumab is
76 the only FDA approved drug for primary progressive MS[13]. Curiously, though,
77 antibody-secreting plasmablasts do not express CD20 (ref [14]). This suggests that
78 the pathogenic role of B cells in MS might lie less with the generation of

79 autoantibodies, and more with their capacity to interact with other immune cell
80 types, such as T cells.

81 Experimental autoimmune encephalomyelitis (EAE) is an animal disease
82 that recapitulates many of the immune aspects of MS pathogenesis. Use of this
83 model has helped us to understand the role of T cells, and $CD4^+$ T cells in
84 particular, in the initiation and maintenance of autoreactive inflammation in the
85 CNS [15]. However, studies using the transgenic $IgH^{[MOG]}$ mouse strain have
86 indicated that B cells may also play a crucial role in EAE pathology[16-18]. These
87 mice (also known as "Th") express a knocked-in IgH chain derived from a MOG-
88 specific antibody; thus, around 30% of their B cells are therefore specific for MOG
89 protein[16]. $IgH^{[MOG]}$ animals develop severe EAE when immunized with either whole
90 MOG protein[16] or with its extracellular domain ($MOG_{[1-125]}$)[19], indicating an
91 important role for MOG-reactive B cells in neuroimmune processes. Further, they
92 develop spontaneous EAE when crossed to myelin peptide-specific T cell receptor
93 transgenic lines on the B6 (ref [17]) and SJL/J[18] backgrounds. Indeed, while "T cell
94 help" is required for the full activation of B cells in the majority of cases, there is
95 increasing evidence that B cells can reciprocally promote effector T cell responses,
96 notably those of the Th17 lineage[20-24]. However, the potential mechanisms by
97 which MOG-reactive B cells facilitate T cell-driven pathogenicity, such as in class
98 II-restricted peptide immunization models of EAE, remain incompletely
99 understood.

100 Here, we studied the co-operative role of B cells and T cells in CNS
101 autoimmunity using $IgH^{[MOG]}$ mice on the non-obese diabetic (NOD) genetic

102 background. We immunized these, and wildtype (WT) NOD mice, with $MOG_{[35-55]}$,
103 a MHC class II-restricted peptide that obligatorily drives a $CD4^+$ T cell response.
104 While WT NOD mice gradually develop a relapsing chronic form of EAE over the
105 course of 80-100 days when immunized with $MOG_{[35-55]}$ [25], we observed that
106 $IgH^{[MOG]}$ mice developed a rapid, severe form of EAE that was characterized by
107 demyelination and inflammation of the CNS. Severe disease in these mice was
108 accompanied by an increase in the frequency of CNS-infiltrating T cells that
109 produced IL-17 and GM-CSF, but not IFNγ; further, the $IgH^{[MOG]}$ CNS meninges
110 was characterized by the presence of colocalized clusters of $CD4^+$ T cells, B cells
111 and $CD11c^+$ dendritic cells (DCs), as well as expansion of the underlying
112 extracellular matrix (ECM) that resembled tertiary lymphoid organs (TLOs).
113 Production of the Th17 maintenance factor IL-23 was increased from CNS-
114 infiltrating B cells in $IgH^{[MOG]}$ mice; *in vivo* blockade of IL-23p19 rescued the severe
115 EAE phenotype in these mice, and also reduced the presence of meningeal TLOs
116 and the frequency of $PD1^+CXCR5^-$ "T peripheral helper-like cells", a recently
117 described effector T cell subset that associates with B cells in the inflamed
118 synovium in rheumatoid arthritis (RA) [26]. Intriguingly, Il23p19 (*Il23a*) transcript
119 expression in the cerebrospinal fluid of MS-affected individuals was correlated to
120 the frequency of B cells. Together, our results demonstrate that MOG-specific B
121 cells play a crucial role in augmenting $CD4^+$ T cell-driven EAE in an IL-23-
122 dependent manner.
123
124 **Results**

125

126 *IgH$^{[MOG]}$ mice develop severe EAE upon active immunization with MOG$_{[35-55]}$*

127

128 When immunized with MOG$_{[35-55]}$, wildtype WT NOD mice display a disease
129 course characterized by relapse remitting disease in the early phase that
130 transitions to a chronic worsening phase in some animals [25]. NOD-EAE has thus
131 been considered a possible model of SPMS [27,28], though others argue against this
132 interpretation [29]. We confirmed that MOG$_{[35-55]}$-immunized WT NOD mice develop
133 disease characterized by relatively mild symptoms over the first ~100 days
134 (Supplemental Figure 1A). We next compared the development of EAE between
135 NOD-background WT and IgH$^{[MOG]}$ mice upon MOG$_{[35-55]}$ immunization. Both male
136 and female IgH$^{[MOG]}$ mice developed extremely severe disease within 25 days
137 (Figure 1A), with a substantial frequency of these mice attaining ethical endpoints
138 (10/14 IgH[MOG] males vs. 0/14 WT males, p=0.0002; 12/16 IgH$^{[MOG]}$ females vs.
139 0/16 WT females, p<0.0001). Histopathological analyses revealed increased
140 lymphocyte infiltration and demyelination in the spinal cords of IgH$^{[MOG]}$ mice
141 relative to controls (Figure 1B).

142 We next examined peripheral T cell responses prior to disease onset. No
143 differences in IL-17 or IFNγ were detected by either *ex vivo* flow cytometry (Figure
144 1C) or by ELISA after MOG$_{[35-55]}$ peptide recall (Supplemental Figure 1B). While
145 the cervical LNs are a potential site of T cell reactivation in MS [30], we observed
146 limited production of IL-17 and IFNγ in this compartment; while a large proportion
147 of CD4^{+} T cells in cervical LNs were positive for TNFα, no differences were

148 detected between WT and IgH$^{[MOG]}$ (Supplemental Figure 1C). To identify a
149 possible role for IgH$^{[MOG]}$ B cells in directly driving T cell responses, we pulsed
150 IgH[MOG] or WT B cells with MOG$_{[35-55]}$ and co-cocultured them with MOG$_{[35-55]}$-
151 specific 1C6 transgenic T cells[31-33]. No differences were observed in T cell
152 proliferation (Supplemental Figure 1D), indicating that IgH$^{[MOG]}$ B cells were not
153 intrinsically better at presenting antigen to T cells.

154 Antigen-specific antibody (Ab) secretion is the primary function of B cells.
155 Further, oligoclonal immunoglobulin (Ig) banding in cerebrospinal fluid (CSF) is an
156 important diagnostic marker for MS [34]. However, no differences in MOG-specific
157 circulating IgG were found in IgH$^{[MOG]}$ serum relative to controls (Figure 1D),
158 suggesting that severe disease in transgenic animals was not accompanied by an
159 increase in MOG-specific autoantibodies. Together, these data showed that the
160 presence of myelin-reactive B cells can exacerbate CNS autoimmunity and tissue
161 damage when EAE is induced in a CD4$^+$ T cell dependent manner. However,
162 increased disease severity was unrelated to increased MOG antibody production
163 or to an increased capacity of IgH$^{[MOG]}$ B cells to facilitate antigen presentation to
164 MOG$_{[35-55]}$-specific CD4$^+$ T cells.

165

166 *Increased presence of immune cells in the CNS of immunized IgH$^{[MOG]}$ mice.*

167

168 Target organ-infiltrating immune cells are essential to the pathogenesis of
169 autoimmune disease. We therefore enumerated the frequency and absolute
170 number of CNS-infiltrating immune cells – CD19$^+$ B cells, CD4$^+$ T cells, CD8$^+$ T

171 cells, CD11c$^+$ dendritic cells (DCs), CD11b$^+$CD11c$^-$ macrophages and Ly6G$^+$
172 neutrophils – in immunized WT and IgH$^{[MOG]}$ mice. The relative frequencies and
173 absolute numbers of CD4$^+$ T cells, CD8$^+$ T cells, DCs, macrophages and
174 neutrophils were significantly increased in the CNS of IgH$^{[MOG]}$ mice relative to WT
175 (Figure 2A).

176 Interestingly, despite having an antigenic repertoire heavily skewed towards
177 MOG reactivity, immunized IgH$^{[MOG]}$ mice did not display an increase in frequency
178 or absolute number (Figure 2A) of B cells in the CNS. We therefore assessed
179 whether there might be differences in the proportion of functional B cell subsets
180 between the groups. Indeed, we observed a stark increase in the frequency of
181 class-switched (CS) IgM$^-$IgD$^-$ B cells in the CNS (Figure 2B) of IgH$^{[MOG]}$ mice, which
182 was accompanied by a decrease in the frequency of immature and mature B cells.
183 In line with our finding that serum MOG-specific IgG was comparable between WT
184 and IgH$^{[MOG]}$, we observed no differences in B cell subpopulation frequency in the
185 spleen (Supplemental Fig 2A). Further, we observed no difference in MHC class II
186 expression between CNS-infiltrating WT and IgH$^{[MOG]}$ B cells (Supplemental Fig
187 2B). On the other hand, an increase in GL-7$^+$Fas$^+$ germinal center (GC) B cells
188 was seen in the IgH$^{[MOG]}$ CNS (Supplemental Figure 2C).

189 B cells can generate canonical inflammatory cytokines such as IL-6 (ref [35]),
190 TNFα [36] and GM-CSF [37], with their production of such cytokines being linked to
191 worsened outcomes in MS. We observed that a significantly greater proportion of
192 IgH$^{[MOG]}$ CNS B cells produced these cytokines as compared to WT counterparts,
193 with the differences in IL-6 and TNFα being most apparent (Fig 2C). Altogether,

194 these data point to qualitative differences between B cells in from the CNS of
195 immunized WT versus IgH$^{[MOG]}$ mice, as well as a quantitative increase of T cells
196 and innate immune cells.
197
198 *Increased frequency of IL-17 and GM-CSF-positive CD4^{+} T cells in IgH$^{[MOG]}$ CNS.*
199
200 As we had observed an elevated frequency of CD4^{+} T cells in the CNS of
201 sick IgH$^{[MOG]}$ mice, we next examined the capacity of these cells to produce
202 inflammatory Th1 and Th17 cytokines by flow cytometry, due to the well-
203 established role of these CD4^{+} effector T cell subsets in EAE [38]. We observed no
204 differences between IgH$^{[MOG]}$ and WT CD4^{+} T cells in their production of the IFNγ
205 and TNFα in the CNS (Figure 3A). By contrast we saw a strong upregulation of IL-
206 17 production from CNS-infiltrating CD4^{+} T cells from IgH$^{[MOG]}$ at disease endpoint.
207 Notably, production of GM-CSF, a key pathogenic cytokine implicated in Th17-
208 driven tissue inflammation, was also augmented in IgH$^{[MOG]}$ CD4^{+} T cells. These
209 findings indicated that Th17 responses were specifically promoted in the CNS of
210 immunized IgH$^{[MOG]}$ mice.
211
212 *Accumulation of meningeal TLOs in IgH$^{[MOG]}$ mice*
213
214 Meningeal TLOs have been documented in progressive MS and their presence
215 correlates with poor outcomes [7,39]. Their presence in EAE is dependent on murine
216 genetic background and the manner of disease induction; while TLOs arise upon

217 active immunization of SJL/J mice with $PLP_{[139-151]}$ [40], they do not appear in $MOG_{[35-55]}$-immunized C57BL/6J mice, rather arising only upon adoptive transfer of Th17 cells [41]. Whether or not they are a feature of NOD-EAE is as-yet unknown. As B cells are crucial to TLO formation[41], we assessed their presence in WT versus $IgH^{[MOG]}$ mice. Strikingly, we observed clustering of $CD4^+$ T cells, B cells and $CD11c^+$ DCs of varying magnitude in the brain and spinal cord of $IgH^{[MOG]}$ relative to WT mice. In the brain, meningeal clustering was chiefly observed in cerebellar fissures (Figure 3B).

TLOs are defined as tissue immune cell aggregates organized within a stroma cell network in inflamed non-lymphoid tissues. We found an increase of elaborate stroma network near the meninges in $IgH^{[MOG]}$ mice as demonstrated by the organized expansion of fibronectin, PDGFRαβa/b IF staining underneath the B cell clustering (Figure 3C). Together, these data demonstrate that TLOs accumulate in the meninges of $MOG_{[35-55]}$-immunized $IgH^{[MOG]}$ mice.

Augmented IL-23 production by $IgH^{[MOG]}$ mice leads to exacerbated disease

Our findings led us to investigate whether $IgH^{[MOG]}$ B cells may be characterized by increased production of the Th17 stabilization factor IL-23, which is essential to Th17 pathogenicity *in vivo* [42,43] and which can be secreted by human B cells[44]. The frequency of B cells co-expressing both chains of IL-23 ($p40^+p19^+$) was strongly upregulated in the $IgH^{[MOG]}$ CNS, despite showing no differences in co-expression of the chains of the related cytokine, and Th1 differentiation factor, IL-12

240 ($p40^+p35^+$) (Figure 4A). Use of an antibody that detected IL-23 heterodimer
241 confirmed that CNS $IgH^{[MOG]}$ B cells show higher expression of this cytokine
242 (Figure 4B). As DCs are considered a major source of IL-23 (ref [45]), we investigated
243 whether their capacity to generate this cytokine differed between WT and $IgH^{[MOG]}$
244 CNS; however, no differences were observed nor between WT and $IgH^{[MOG]}$
245 astrocytes[46] or microglia (Supplemental Figure 3A).

246 The robust upregulation of IL-23 by B cells in the $IgH^{[MOG]}$ CNS led us to ask
247 whether it might be essential for the exacerbated disease seen in these animals.
248 We therefore actively immunized $IgH^{[MOG]}$ mice and administered either anti-IL-
249 23p19 blocking antibody[47] or isotype control. *In vivo* blockade abrogated severe
250 EAE (Figure 4C), characterized by reduced lymphocyte infiltration and
251 demyelination in the spinal cord (Figure 4D). Further, CNS-infiltrating $CD4^+$ T cells
252 from anti-p19-treated $IgH^{[MOG]}$ mice showed decreased IL-17, and a trend towards
253 reduced GM-CSF expression (Figure 4E); however, no differences in IFNγ
254 production between T cells from anti-19 or isotype-treated mice were observed. In
255 sum, these data show that excessive production of IL-23 by $IgH^{[MOG]}$ may underpin
256 the severe pathology observed in these animals.

257

258 *T peripheral helper (Tph)-like cells accumulate in the $IgH^{[MOG]}$ CNS*

259

260 T follicular helper (Tfh) cells play a critical role in germinal center formation and B
261 cell immune activation, and were recently shown to collaborate with B cells in
262 driving Th17-dependent EAE [48]. We therefore examined the presence of PD-

263 1^{+}CXCR5^{+} Tfh cells in splenic and CNS tissues from WT and IgH$^{[MOG]}$ mice. Tfh
264 were relatively rare in all cases (Figure 5A). Intriguingly, we instead observed a
265 increase in PD-1^{+}CXCR5^{-} CD4^{+} T cells in the IgH$^{[MOG]}$ CNS (Figure 5A). These
266 cells were reminiscent of the recently discovered "T peripheral helper" (Tph) cell
267 subset [26,49]. Originally discovered in the context of rheumatoid arthritis (RA), Tph
268 are recruited to the inflamed synovium, where they associate with B cells. They
269 are distinct from Tfh[26], and indeed we found that PD-1^{+}CXCR5^{-} cells from both WT
270 and IgH$^{[MOG]}$ mice were negative for the Tfh master transcription factor Bcl6 (ref [50];
271 Supplemental Figure 4A). While present in human RA [26,49] and lupus [51], evidence
272 for the accumulation of Tph in murine autoimmune disease is, thus far, limited.
273 Interestingly the frequency of PD-1^{+}CXCR5^{-} CD4^{+} T cells was higher at the peak
274 of EAE in IgH$^{[MOG]}$ mice as opposed to at onset or recovery (Figure 5B).

275 In addition to being PD-1^{+}CXCR5^{-}Bcl6^{-}, Tph are characterized as highly
276 positive for ICOS, CXCL13 and IL-21 (ref [26]). We therefore compared expression
277 of these markers between CNS-infiltrating PD-1^{neg} and PD-1^{+} CD4^{+} T cells of both
278 WT and IgH$^{[MOG]}$ mice. Expression of all three markers was upregulated in the PD-
279 1^{+} subpopulation in both WT and IgH$^{[MOG]}$ (Figure 5C), showing that CNS-
280 infiltrating PD1^{+}CXCR5^{-} cells express known Tph markers in the context of NOD-
281 EAE. By contrast, there was no difference in Bcl6 expression between PD-1^{+} and
282 PD-1^{-} cells (Supplemental Figure 4B) Interestingly, expression of IL-21 was
283 significantly higher in IgH$^{[MOG]}$ Tph-like cells relative to WT (Figure 5D). Altogether,
284 our data indicate that Tph-like cells accumulate in the CNS of EAE animals in the
285 presence of MOG-specific B cells.

286

287 *IL-23 is required for TLO formation and Tph recruitment*

288 As Th17 cells are crucial to TLO formation[41], and as we had shown that the
289 Th17 lineage maintenance factor IL-23 is obligatory for severe EAE in IgH$^{[MOG]}$
290 mice (Figure 4C), we next examined the effects of IL-23 blockade on the presence
291 of TLOs in the meninges. Administration of anti-IL23p19 diminished the number of
292 lymphocyte clusters in the meninges of IgH$^{[MOG]}$ mice (Figure 6A). Concomitantly,
293 we observed a decrease in the intricate ECM network underneath, suggesting a
294 decrease in meningeal TLOs in IgH$^{[MOG]}$ mice after administration of anti-IL23p19
295 (Figure 6B). We next examined whether *in vivo* depletion of IL-23 could impact Tph
296 frequency. Indeed, the frequency of Tph was reduced in the CNS, but not spleen,
297 of immunized IgH$^{[MOG]}$ treated with anti-p19 (Figure 6C). Therefore, we concluded
298 that expression of IL-23 in IgH$^{[MOG]}$ underpinned not only severe disease, but also
299 meningeal inflammation as well as recruitment of Tph to the CNS.

300

301 *IL-23 expression in MS CSF correlates with the presence of B cells*

302 The cerebrospinal fluid is a useful proxy for pathologic processes within the
303 CNS parenchyma[52] and is routinely sampled in MS diagnosis. We therefore asked
304 whether expression of IL-23p19 transcript in the CSF of MS-affected individuals
305 were altered in relation to the presence of B cells. We examined the CSF of 11 MS
306 patients for expression of *Il23a* (IL-23p19 gene name) and correlated this to the
307 frequency of CD19^{+} B cells in the CSF of the same individuals. A robust correlation

308 was identified (Spearman r = 0.7107) between *IL23a* and the proportion of $CD45^+$
309 leukocytes that were $CD19^+$ (Fig. 6D).
310
311 **Discussion**
312
313 The role of $CD4^+$ T cells in the autoimmune pathogenesis of MS is well-established:
314 genome-wide association studies (GWAS) have revealed that polymorphisms in
315 the human leukocyte antigen class II region are strongly associated with MS
316 susceptibility [53], and many of the current treatments of MS are believed to target T
317 cell responses [54-56]. However, the success of the B cell-depleting drug ocrelizumab
318 in both RRMS and PPMS has intensified recent interest in the contribution of B
319 cells to disease processes [57].
320 $IgH^{[MOG]}$ mice were initially described on the C57BL/6 (B6) and SJL/J
321 genetic backgrounds. On the B6 background, $IgH^{[MOG]}$ mice showed an increased
322 incidence of EAE, relative to WT, when immunized with whole MOG protein[16].
323 Notablyly, $IgH^{[MOG]}$ SJL/J mice developed EAE of greater severity than controls
324 when immunized with the myelin-derived epitope proteolipid protein $(PLP)_{[139-154]}$[16],
325 which induces a relapsing/remitting disease pattern in SJL/J background mice[58].
326 This suggested that the presence of MOG-reactive B cells could contribute to EAE
327 pathology that was driven by a class II-restricted peptide. It was later shown that
328 when $IgH^{[MOG]}$ mice were crossed to the 2D2 $MOG_{[35-55]}$ TcR-transgenic strain on
329 the C57BL/6 background, the resulting double-transgenics spontaneously
330 developed Devic's-like disease while single transgenic mice did not[17]. Similarly,

331 IgH$^{[MOG]}$ x TCR^{1640} (ref [18]) and IgH$^{[MOG]}$ x 1C6 (ref [31]) double-transgenic mice, on
332 the SJL/J and NOD backgrounds respectively, develop spontaneous EAE at a high
333 rate of incidence[31]. These findings indicated that the collaboration of both myelin-
334 specific B and T cells in the same animal could induce CNS autoimmunity;
335 however, it was difficult to determine whether B or T cell-driven responses were
336 initially responsible for disease induction in this model, and thus the nature of a
337 putative collaboration between B cells and T cells in disease processes remained
338 incompletely defined.

339 In our study, we actively immunized IgH$^{[MOG]}$ mice on NOD background with
340 the class II-restricted peptide MOG$_{[35-55]}$. This permitted us to study the contribution
341 of MOG-reactive B cells in a model of EAE that is initiated by CD4^{+} T cells. While
342 WT NOD mice developed a gradual, chronic MOG$_{[35-55]}$-driven disease course, with
343 advanced symptoms appearing as late as >100 days post immunization, we found
344 that immunized IgH$^{[MOG]}$ NOD mice develop severe disease within a matter of
345 weeks. Thus, by using a myelin-derived, class II-restricted, immunogen, we show
346 that B cells augment EAE even when CD4^{+} T cells initiate disease. Interestingly,
347 no differences in circulating anti-MOG IgG were identified between immunized
348 between WT and IgH$^{[MOG]}$, suggesting that worsened disease in IgH$^{[MOG]}$ mice is
349 not the result of increased production of encephalitogenic autoantibody.

350 The role of CD4^{+} T cells in licensing peripheral B cell responses is well-
351 established, and indeed the term “helper T cell” is derived from this function[59].
352 Th17 cells, in particular, can foster B cell responses by inducing class switching to
353 inflammatory IgG1 and IgG2a[60] and by recruiting B cells to TLO structures[61]. Here,

354 we provide evidence that the converse is also true, and that B cells may
355 themselves shape Th17 responses. CNS-infiltrating $CD4^+$ T cells in $IgH^{[MOG]}$ mice
356 showed significantly higher expression of IL-17 and GM-CSF, but not of IFNγ,
357 indicating that Th17 responses are elevated in these mice. Further, CNS-infiltrating
358 $IgH^{[MOG]}$ B cells showed increased expression of IL-23, an innate immune-
359 associated cytokine that stabilizes the Th17 lineage and is required for the
360 pathogenicity of Th17 cells[42,43], and *in vivo* blockade of IL-23 sharply reduced EAE
361 in $IgH^{[MOG]}$ mice.

362 Overall, our findings show that B cells can play an important supportive role
363 in facilitating pathogenic Th17 function and are consistent with a model by which
364 bidirectional B:Th17 interactions are essential in CNS autoimmunity. Indeed, there
365 is emerging evidence that B cells can promote Th17 responses. Both peritoneal
366 $CD5^+B220^{lo}$ (ref [20]) and LPS-stimulated splenic $CD80^+CD86^+CD44^+$ (ref [21]) B cells
367 can elicit Th17 differentiation. Further, production of IL-17 is defective from T cells
368 taken from agammaglobulinemia patients that lack B cells[22] and therapeutic
369 depletion of B cells with rituximab can reduce Th17 function in the context of MS[23]
370 as well as in rheumatoid arthritis[24]. The mechanisms underpinning bidirectional B
371 cell: T cell interactions remain to be fully elucidated.

372 Human B cells can secrete IL-23, and repression of this capacity is posited
373 as a mechanism of action for interferon-beta in MS[44]. It was previously observed
374 that peripheral B cells from naïve $IgH^{[MOG]}$ mice possess the capacity to secrete IL-
375 23 (ref [62]); both upon pulsing with rMOG, and most strikingly upon co-culture with
376 $MOG_{[35-55]}$-specific 2D2 T cells in the presence of either rMOG or $MOG_{[35-55]}$. B cell

377 production of IL-23 in response to LPS is repressed by the inhibitory receptor Tim-
378 1 (ref [63]). We now show that immunization with $MOG_{[35-55]}$ elicits IL-23 expression
379 from CNS-infiltrating B cells *in vivo*, and that IL-23 is essential to both EAE and
380 TLO formation from these animals.

381 Using mass cytometry, Brenner and colleagues found that $PD1^{+}CXCR5^{-}$
382 $CD4^{+}$ T cells accumulate in the inflamed synovium of RA patients. These Tph cells
383 secrete B cell attractant factors such as CXCL13 and IL-21 and associate with B
384 cells in the inflamed synovium, both in defined lymphoid aggregates as well as
385 more diffusely. However, in contrast to Tfh cells, Tph are not defined by expression
386 of the transcription factor Bcl6 [26]. While these cells are also observed in patients
387 with lupus[51] and ANCA-associated vasculitis[64], their potential roles in murine
388 models of autoimmunity remain obscure. We have found an enrichment of
389 $PD1^{+}CXCR5^{-}$ $CD4^{+}$ T cells in the CNS, but not immune periphery, of immunized
390 $IgH^{[MOG]}$ mice. These cells are $Bcl6^{neg}$ and show increased expression of the Tph
391 markers ICOS, CXCL13 and IL-21, relative to $PD\text{-}1^{-}$ counterparts. Intriguingly, we
392 find that the presence of $PD\text{-}1^{+}CXCR5^{-}$ cells is highest in mice of peak EAE
393 severity; Tph cells were previously shown to correlate with the severity of
394 rheumatoid arthritis [26] and lupus [51]. Further, the accumulation of Tph cells in the
395 CNS is dependent on IL-23, revealing a heretofore unknown function of this
396 cytokine.

397 In conclusion, we provide evidence that in the presence of a B cell repertoire
398 that is skewed towards MOG, NOD-background mice develop unusually rapid and
399 severe $CD4^{+}$ T cell-mediated EAE. Disease is dependent on IL-23, which is

400 produced by B cells and is required for the augmented Th17 responses seen in
401 these mice. Furthermore, these mice show accumulation of TLOs in their
402 meninges that are again dependent on the presence of IL-23. Together, our
403 findings support a critical role for myelin-reactive B cells in bolstering T cell-driven
404 CNS autoimmunity in an IL-23-dependent manner.
405
406 **Methods**
407 *Ethics*
408 All mouse experiments and breedings were approved by the Animal Protection
409 Committee of Université Laval (protocols 2021-820 and 2021-830, to M.R).
410 Protocols and experiments involving human participants were approved by the
411 Newfoundland Health Research Ethics Board (to C.S.M).
412
413 *Animals*
414 IgH$^{[MOG]}$ mice on the NOD background[31], and 1C6 mice[31-33], were obtained from
415 Dr. Vijay Kuchroo (Brigham & Women's Hospital, Boston), and were maintained at
416 the animal facility of the Centre de recherche du CHU de Québec-Université Laval.
417 NOD/ShiLtJ and NOD.*Scid* mice were purchased from Jackson Laboratories.
418
419 *EAE induction and scoring*
420 WT NOD and IgH$^{[MOG]}$ mice were immunized subcutaneously with 200µg MOG$_{[35-}$
421 $_{55]}$ (Feldan), emulsified in incomplete Freund's adjuvant (BD Difco) that was
422 supplemented with 500 µg *M. tuberculosis* extract (BD Difco). On day 0 and day 2

423 post-immunization, mice received 200 ng pertussis toxin (List Biological
424 Laboratories) intraperitoneally. Mice were monitored daily for signs of EAE, which
425 were assessed using a semi-quantitative 0-5 scale: 0; no disease, 0.5; ruffled fur,
426 1; limp tail, 1.5; mild impairment in gait, 2; severe impairment in gait, 2.5; partial
427 hind limb paralysis, 3; hind limb paralysis, 4; forelimb paralysis, 5; moribund [65].
428 Pre-onset analyses were conducted a minimum of 5 days post-immunization but
429 before the onset of symptoms. For comparison of disease burden, area under
430 curve was calculated for individual disease curves and was divided by the number
431 of days in the protocol (AUC d^{-1}). For p19 blockade, mice were administered anti-
432 p19 (clone G23-8) or istotype (rIgG1, clone HRPM; both BioXcell), 1 mg d^{-1} on d -
433 1 and d6 [47].
434
435 *Histopathology*
436 Mice were euthanized and intracardially perfused with PBS. The spinal cord was
437 extracted and fixed in 10% formalin and 30% sucrose prior to being embedded in
438 paraffin. Five-to-seven-micron coronal sections of the spinal cords were collected
439 on superfrost microscope slides (using microtome, Leica Biosystems HistoCore
440 Autocut) and dried overnight on a drying bench at 37°C. Slides were stored at room
441 temperature in a slide storage box until staining was performed. Sections for
442 Hematoxylin and Eosin (H&E) were deparaffinated with xylene, while toluene was
443 used for Luxol Fast Blue (LFB) sections. Histology was performed as previously
444 described [66], using standard H&E to visualize lymphocyte infiltration and LFB to
445 stain myelin in order to visualize areas of demyelination. Briefly, stained slides

446 were scanned at 20x using a brightfield microscope scanner (Aperio AT2 DX
447 System), and representative RGB images of the cervical spine were acquired.
448 Quantification of the staining was performed on Image J (software, v 1.53K) in a
449 blinded manner. Images were split into separate single colour channels using the
450 Colour Deconvolution plugin. Thresholding was performed on the single colour
451 channels for hematoxylin and LFB, and an area fraction measurement was
452 performed on the white matter of the spinal cord. Staining is expressed as the
453 percent of total white matter that is stained.
454
455 *Immunofluorescence*
456 Immunofluorescence (IF) analysis was performed on flash-frozen brain tissue
457 embedded in optimum cutting temperature medium (OCT). The tissue was cryo-
458 sectioned (7-10um) and mounted onto positively charged slides. IF staining were
459 performed with antibodies against surface immune antigens such as CD4, B220,
460 CD45 and CD11c and in some cases against ECM antigens: Fibronectin,
461 PDGFRα/β simultaneously. Slides were imaged using a widefield inverted
462 microscope (AxioObserver 7) and analysis was done using Image J software.
463
464 *ELISA*
465 Splenocytes and draining lymph nodes were isolated from NOD and IgH$^{[MOG]}$ mice
466 5d post-immunization. Cells were cultured at a concentration of 10×10^6 cells mL^{-}
467 ^{1} in T cell media and stimulated, or not, with 10 mg mL^{-1} MOG$_{[35-55]}$. Supernatants
468 were collected at d5 of the culture for the analysis of T cell cytokine production

469 using a combination of commercially available antibodies (Biolegend). Briefly, the
470 capture antibodies used were: purified anti-mouse IFNg (clone R4-6A2)
471 and purified anti-mouse IL-17 (clone TC11-18H10.1). The detection antibodies
472 used were: biotin anti-mouse IFNg; clone XMG1.2, biotin anti-mouse IL-17;
473 clone TC11-8H4. Following the incubation with the avidin-horseradish peroxidase
474 (Biolegend) and TMB substrate (Mendel Scientific), colorimetric readings were
475 performed using a SpectraMax i3 Microplate Reader.
476
477
478 *Measurement of serum immunoglobulin*
479 Blood was collected from Igh[MOG] mice and WT mice at endpoint. Serum was
480 collected by centrifuging blood samples at 2000g for 10min. Total anti-MOG IgG
481 was quantified by using SensoLyte Anti-Mouse MOG(1-125) IgG Quantitative
482 ELISA Kit (Anaspec).
483
484 *Isolation of CNS-infiltrating mononuclear cells*
485 Mice were euthanized and perfused intracardially with PBS. Brain and spinal cord
486 were dissected from the skull and vertebral column respectively and were prepared
487 as previously described [65]. Briefly, CNS tissues were digested with liberase
488 (Roche) and DNAse I (Sigma) and cells were enriched using a 35% Percoll (GE
489 Healthcare) gradient.
490
491 *Flow cytometry*

492 Single cell suspensions were obtained from spleens, lymph nodes and CNS of
493 EAE mice. For detection of surface antigens, cells were stained with Fixable
494 Viability Dye (eBioscience) and incubated with Fc Block (Biolegend) prior to
495 staining with antibodies against surface antigens (CD45, CD4, CD8, CD19,
496 CD11b, CD11c, B220, Ly6G, IgD, IgM, FAS, GL7, PD-1, CXCR5, ICOS, I-Ag^7,
497 GFAP; details in following section). For detection of intracellular cytokines, cells
498 were first stimulated with 50ng ml^{-1} PMA (Sigma), 1μM ionomycin (Sigma) and 1μL
499 mL^{-1} GolgiStop (BD) for 4 hours at 37°C, prior to being labeled with viability
500 indicator, Fc Block and relevant surface antigens as above. They were then fixed
501 and permeabilized (Fixation Buffer and Intracellular Staining Perm Wash Buffer,
502 both Biolegend) and stained for intracellular markers (IFN-γ, IL-17A, TNF-α, IL-6,
503 GM-CSF, IL-12p40, IL-12p35, IL-23p19, IL-23; Bcl6, IL-21, CXCL13; details in
504 following section). Samples were analyzed on a FACS Aria (BD) and data were
505 analyzed using FlowJo software (Treestar).
506
507 *Flow cytometry antibodies*
508 The following monoclonal antibodies against mouse antigens were used: CD45,
509 clone A20 (Biolegend); CD11b, clone M1/70 (eBioscience); CD11c, clone N418
510 (Biolegend); Ly6G, clone 1A8 (BD Biosciences); CD4, clone RM4-5 (eBioscience);
511 CD8, clone 53-6.7 (Biolegend); CD19, clone 1D3 (eBioscience); B220, clone RA3-
512 6B2 (eBioscience); IgD, clone 11-26c (eBioscience); IgM, clone 11/41
513 (eBioscience); FAS, clone 15A7 (eBioscience); GL7, clone GL-7 (eBioscience);
514 PD-1, clone J43 (eBioscience), CXCR5, clone SPRCL5 (eBioscience); ICOS,

515 clone C398.4A (eBioscience); GFAP, clone 1B4 (BD Biosciences); I-Ag^7, clone 39-
516 10-8 (Biolegend); IFN-γ, clone XMG1.2 (eBioscience); TNF-α, clone MP6-XT22
517 (eBioscience); IL-17a, clone TC11-18H10.1 (Biolegend); GM-CSF, clone MP1-
518 22E9 (eBioscience); IL-6, clone MP5-20F3 (eBioscience); IL-21, clone mhalx21
519 (eBioscience); IL-23 heterodimer, clone IC18871P (R&D Systems); IL-23p19,
520 clone fc23pg (eBioscience); IL-12p35, clone 4D10p35 (eBioscience); IL-12p40,
521 clone C17.8 (eBioscience); BCL6, clone IG191E/A8 (eBioscience); CXCL13, clone
522 D58CX13 (eBioscience).
523
524 *Immunofluorescence antibodies*
525 The following monoclonal antibodies against mouse antigens were used: CD4
526 (RM4-5), B220 (RA3-6B2), CD11c (N418), CD45.2 (104), PDGFRα (APA5), and
527 PDGFRβ (APB5), all of which are from eBioscience; and fibronectin (GW20021F,
528 Sigma); smooth muscle actin (1A4, Sigma).
529
530 *Antigen presentation assay*
531 Single cell suspensions were obtained from the spleens of unimmunized WT and
532 IgH[MOG] mice. Cells were labeled with CD43 (Ly-48) Microbeads (Miltenyi), and
533 $CD43^+$ leukocytes (all leukocytes except resting B cells) were depleted on a
534 magnetic MACS column (Miltyeni). Unlabelled $CD43^-$ cells were collected and
535 were subsequently stained with anti-mouse CD19. $CD19^+$ B cells were purified
536 using high-speed cell sorting. In parallel, $CD4^+$ T cells were purified from the
537 spleens of 1C6 mice using mouse CD4 MicroBeads (Miltenyi) and labeled with

538 CellTrace Violet (CTV; Thermo Fisher Scientific). CTV-labeled 1C6 $CD4^+$ T cells
539 were cultured with B cells at a ratio of 1 CD4: 1 B, with 0, 1 or 10µg ml^{-1} $MOG_{[35-}$
540 $_{55]}$ for 72 hours. CTV dilution was assessed by flow cytometry.
541
542 *Tfh culture*
543 The protocol of Gao et al was adapted[67]. Briefly, $5x10^5$ splenocytes from NOD mice
544 were stimulated 24h with LPS (1 µg mL^{-1}). $1x10^4$ $MOG_{[35-55]}$-specific 1C6
545 $CD4^+CD62L^{hi}$ T cells were then plated on top of the splenocytes with 1µg mL^{-1}
546 $MOG_{[35-55]}$, plus 50 ng ml^{-1} IL-21 and 100 ng mL^{-1} of IL-6 (Tfh) or no additional
547 cytokines (Th0) for 72h.
548
549 *Analysis of CSF from MS-affected individuals*
550 5mL of CSF was collected from consenting adult participants with MS at The
551 Health Sciences Centre neurology clinic in St. John's, NL between July 2021 and
552 May 2022. For CSF immune phenotyping, 2.5mL of CSF was centrifuged for 10
553 minutes at 300g and the CSF was removed. The CSF cell pellet was resuspended
554 in 100uL of flow buffer (1% bovine albumin serum, 2mM EDTA, 2mM sodium azide
555 in PBS). The CSF cell suspension was added to a DURAclone IM Phenotyping
556 BASIC tube (Beckman Coulter), mixed and incubated at 4°C for 30 minutes. The
557 cells were washed with 4mL flow buffer, centrifuged at 300g for 5 minutes,
558 decanted and resuspended in 100µL 2% paraformaldehyde. Data was acquired
559 from the whole sample using a Cytoflex flow cytometer (Beckman Coulter) and

560 analysed using FlowJo software. The $CD19^+$ cell count was expressed as a
561 percentage of the total number of $CD45^+$ cells.
562
563 For measurement of CSF cell *Il23a* expression, 2.5 mL of human CSF was
564 centrifuged at 300g for 10 minutes and the CSF supernatant was carefully
565 removed. The CSF cell pellet was resuspended in 500ul of Trizol and stored at -
566 80°C. Total RNA was extracted using chloroform extraction followed by an RNeasy
567 Micro kit (Qiagen). 200ng of RNA was used to synthesize cDNA with the M-MLV
568 Reverse Transcriptase kit (Invitrogen). *Il23a* transcript expression was quantified
569 using *Il23a* (FAM labelled) and GAPDH (VIC labelled) Taqman probe/primer
570 assays (Invitrogen), Fast Advanced Master mix (Invitrogen) and a ViiA7 Real-time
571 PCR system (Applied Biosystems).
572
573 *Statistical analysis*
574 Comparisons between two groups were made by *t*-test. Fisher's exact test was
575 used to test for differences in the frequency of mice attaining ethical endpoints. For
576 calculation of Tph frequency at different disease stages, Tukey's multiple
577 comparisons test was used. Two-tailed analyses were used in all instances. All
578 statistical analyses were conducted using Prism software (GraphPad).
579
580
581
582

583 **Abbreviations**

584

585 Ab, antibody; CNS, central nervous system; CSF, cerebrospinal fluid; CTV,
586 CellTrace Violet; DC, Dendritic cell; EAE, experimental autoimmune
587 encephalomyelitis; EP, endpoint; GC, Germinal center; GM-CSF, granulocyte and
588 macrophage colony stimulating factor; H&E, hematoxylin & eosin; IFN, interferon;
589 Ig, immunoglobulin; IL, interleukin; LFB, Luxol fast blue; MHC, major
590 histocompatibility complex; MOG, myelin oligodendrocyte glycoprotein; MS,
591 multiple sclerosis; NOD, nonobese diabetic; PLP, proteolipid protein; preonset,
592 PO; RR, relapsing/remitting; SP, secondary progressive; Tfh, T follicular helper;
593 TLO, Tertiary lymphoid organ; TNF, tumor necrosis factor; Tph, T peripheral
594 helper; WT, wildtype.

595

596

597 **Declarations**

598

599 *Competing interests*

600 M.R. held a research contract with Remedy Pharmaceuticals (2019-2020), with
601 funds paid to the CHU de Québec. This contract is unrelated to the work in this
602 manuscript.

603

604 *Funding*

605 The work was supported by a Biomedical Discovery Research Grant from the MS
606 Society of Canada (#3781) and a CIHR Project Grant, to MR. RF and PG are
607 supported by Ph.D. studentships from the Fonds recherche du Québec – Santé
608 (FRQS). PMIAD was supported by a doctoral studentship from the Multiple
609 Sclerosis Society of Canada. NB is Junior-2 scholar, and MR is a Senior scholar,
610 of the FRQS.

611

612 *Authors' contributions*

613 RF directed the project conducted experiments and helped write the manuscript.
614 PMIAD, NF, IA, APY and JB conducted experiments. RP, AR, BM, SL and OR
615 conducted histological analyses. PG and NB assisted with serum detection of
616 immunoglobulins. CSM contributed to writing of the manuscript. MR supervised
617 the project and wrote the manuscript. All authors read and approved the final
618 manuscript.

619

620 *Acknowledgements*

621 We thank Vijay Kuchroo for providing us with NOD-background IgH$^{[MOG]}$ and 1C6
622 mice respectively. We thank Françoise Morin for critical discussions; Vincent
623 Desrosiers, Alexandre Brunet, Stéphanie Fiola for technical assistance with flow
624 cytometry; and Kim Larose, Andrée Brisson, Mathieu Vallière-St-Amant, Cindy
625 Ouellet and the veterinary service of Université Laval for technical assistance and
626 collaboration regarding animal care.

627

628 **Figure legends**

629

630 **Figure 1. Active immunization with $MOG_{[35-55]}$ induces severe EAE in $IgH^{[MOG]}$**
631 **mice. A.** *Left,* Disease curves and linear regression of males (WT, n=10, $IgH^{[MOG]}$,
632 n=10) and females (WT, n=10, $IgH^{[MOG]}$, n=10) immunized with $MOG_{[35-55]}$ and
633 monitored for development of EAE. ****, p<0.0001. Representative of 2
634 experiments in each sex. *Right*, AUC analysis of disease curves for all mice studied
635 (30 WT, 30 $IgH^{[MOG]}$). **B.** WT and $IgH^{[MOG]}$ spinal cords were sectioned and stained
636 with hematoxylin & eosin (H&E; immune infiltration) and Luxol fast blue (LFB;
637 myelin). Slides were canned at 10X magnification for quantification. WT, n=3,
638 $IgH^{[MOG]}$, n=3. *, p<0.05, *t*-test. **C.** WT (n=3) and $IgH^{[MOG]}$ (n=3) mice were
639 immunized with $MOG_{[35-55]}$. LN cells were isolated at disease onset and IFNγ and
640 IL-17 expression were determined by flow cytometry. Gated on live $CD4^+CD44^+$
641 events. **D.** Sera were collected from $MOG_{[35-55]}$-immunized WT (n=5) and $IgH^{[MOG]}$
642 (n=5) mice, and concentration of MOG-specific IgG was assessed by ELISA. n.s.,
643 not significant; *t*-test. *, p<0.05; ****, p<0.0001; n.s., not significant; linear
644 regression analysis (**A**), *t*-test (**A-D**).

645

646 **Figure 2. Increased presence of class-switched and inflammatory cytokine-**
647 **positive B cells in the $IgH^{[MOG]}$ CNS. A.** Mononuclear cells were isolated from the
648 CNS of immunized WT (n=6) and $IgH^{[MOG]}$ (n=12) mice. Frequency and absolute
649 numbers of $CD19^+$ B cells, $CD4^+$ and $CD8^+$ T cells, $Ly6G^+$ neutrophils,
650 $CD11b^+CD11c^-$ macrophages and $CD11c^+$ dendritic cells were enumerated by flow

651 cytometry. **B.** The frequency of immature ($IgM^{mid}IgD^{mid}$), mature ($IgM^{hi}IgD^{hi}$) and
652 class-switched (CS; $IgM^{-}IgD^{-}$) B cells were assessed from WT (n=5) and $IgH^{[MOG]}$
653 (n=5) CNS. Gated on live $B220^{+}$ events. **C.** Expression of the indicated cytokines
654 was assessed from WT (n=5) and $IgH^{[MOG]}$ (n=5) CNS B cells. Gated on live $CD19^{+}$
655 events. *, p<0.05; **, p<0.01; ***, p<0.001; ****, p<0.0001; n.s., not significant; *t*-
656 test.
657
658 **Figure 3. $IgH^{[MOG]}$ B cells exacerbate CNS-specific Th17 responses and show**
659 **accumulation of meningeal TLOs. A.** WT (n=5) and $IgH^{[MOG]}$ (n=5) were
660 immunized with $MOG_{[35-55]}$ and CNS-infiltrating $CD4^{+}$ T cells were isolated at
661 endpoints. Expression of the indicated cytokines was assessed by intracellular flow
662 cytometry. Gated on live $CD4^{+}$ events. *, p<0.05; **, p<0.01; n.s., not significant; *t*-
663 test. **B.** Brain and spinal cord meningeal sections from $MOG_{[35-55]}$-immunized WT
664 (n=3) or $IgH^{[MOG]}$ (n=3) mice were assessed by immunofluorescence (IF) for
665 expression of B220 (red), CD4 (blue), and CD11c (green), and lymphocyte
666 aggregates from the cerebellar meningeal compartment were enumerated. **C.**
667 Assessment of the ECM near meninges in the cerebellum was determined by IF.
668 Expansion on the meningeal ECM is shown by fibronectin (green) and
669 PDGFRα/β (blue) which overlap with B220 B cell clusters. Dotted lines outline the
670 meningeal membrane and (*) denotes vascular endothelium.
671
672 **Figure 4. CNS $IgH^{[MOG]}$ B cells upregulate IL-23. A.** WT (n=10) and $IgH^{[MOG]}$
673 (n=10) mice were immunized with $MOG_{[35-55]}$ and B cells were isolated from CNS

674 tissues at endpoints. Expression of IL-12p35, IL-12p40 and IL-23p19 were
675 assessed by intracellular flow cytometry. **B.** NOD (n=6) and IgH$^{[MOG]}$ (n=6) mice
676 were immunized with MOG$_{[35-55]}$ and B cells were isolated from CNS tissues at
677 endpoints. Expression of IL-23 heterodimer was assessed by intracellular flow
678 cytometry. **C.** IgH$^{[MOG]}$ mice were immunized with MOG$_{[35-55]}$ and were treated on
679 d (-1) and d6 with 1 mg anti-p19 (n=5) or rIgG1 isotype (n=5). Disease curves
680 representative of 3 experiments. AUC calculations include all mice studied; anti-
681 p19 (n=14) or rIgG1 isotype (n=14). **D.** Inflammatory foci (H&E) and demyelination
682 (LFB) were quantified from cervical spine of immunized IgH$^{[MOG]}$ mice treated with
683 anti-p19 (n=3) or rIgG1 isotype (n=3). **E.** IL-17 and IFNγ were assessed from CNS-
684 infiltrating CD4^{+} T cells of mice from (**C**). *, $p<0.05$; **, $p<0.01$; ***, $p<0.001$; n.s.,
685 not significant; *t*-test.
686
687 **Figure 5. Tph cells infiltrate the IgH$^{[MOG]}$ CNS. A.** WT (n=6) and IgH$^{[MOG]}$ (n=6)
688 mice were immunized with MOG$_{[35-55]}$ and T cells were isolated from spleen and
689 CNS at endpoints. Expression of PD-1 and CXCR5 was assessed by flow
690 cytometry. **B.** WT or IgH$^{[MOG]}$ mice were immunized and sacrificed at onset (n=4
691 each), peak (n=3 each), recovery (n=3 each). CNS-infiltrating CD4^{+} T cells were
692 isolated from these groups, as well as from mice that did not develop disease (n=4
693 each) and the frequency of PD-1^{+}CXCR5^{-} cells was assessed. **C.** Expression of
694 IL-21, CXCL13 and ICOS was assessed from CNS-infiltrating CD4^{+} T cells taken
695 from immunized WT (n=6) and IgH$^{[MOG]}$ (n=6) mice, and expression between PD-
696 1^{-} and PD-1^{+} CD4^{+} subpopulations was compared. **D**. Expression of IL-21, was

697 compared between WT and IgH$^{[MOG]}$ CNS-infiltrating CD4^{+} T cells using the same
698 samples as in (**C**). *, p<0.05; **, p<0.01; ***, p<0.001; ****, p<0.0001; n.s, not
699 significant; unpaired *t*-test (**A**, **D**), Tukey's multiple comparisons test (**B**), paired *t*-
700 test (**C**).
701
702 **Figure 6. Tertiary lymphoid organs accumulate in the meninges of IgH$^{[MOG]}$**
703 **mice in an IL-23-dependent manner.** IgH$^{[MOG]}$ mice were immunized with MOG$_{[35-}$
704 $_{55]}$ and were treated on d -1 and d6 with 1 mg anti-p19 or rIgG1 isotype. **A.**
705 Cerebellar meningeal sections from MOG$_{[35-55]}$-immunized IgH$^{[MOG]}$ mice, treated
706 with isotype (n=6) or anti-p19 (n=6), were assessed for lymphocyte clusters. **B.**
707 ECM deposition underneath meningeal lymphoid aggregates were assessed as in
708 **Fig. 3C**. **C.** T cells were isolated from spleen and CNS at endpoints from anti-p19
709 (n=5) or isotype-treated (n=5) mice. Expression of PD-1 and CXCR5 was
710 assessed by flow cytometry. **D.** *Il23a* was assessed from CSF immune cells of MS-
711 affected individuals (10 RRMS, 1 PPMS) by qPCR and was correlated to the
712 frequency of CD19^{+} B cells within the CD45^{+} CSF leukocyte population of each
713 patient. *, p<0.05; **, p<0.01. *t*-test (**A, C**); linear regression (**D**).
714
715 **Supplemental Figure 1. A.** WT NOD mice (n=5) were immunized with MOG$_{[35-55]}$
716 and were monitored for signs of EAE for 120d. **B.** Splenic and LN cells were
717 isolated from immunized WT (n=3) and IgH$^{[MOG]}$ (n=3) cells at disease onset, and
718 were stimulated with 10 μg mL^{-1} MOG$_{[35-55]}$. Supernatants were collected at d5 and
719 IFNγ and IL-17 were assessed by ELISA. **C.** WT (n=8) and IgH$^{[MOG]}$ (n=8) mice

720 were immunized with $MOG_{[35-55]}$, and $CD4^+$ T cells were isolated from cervical LNs
721 at endpoints and assessed for expression of the indicated cytokines. **D.** WT or
722 $IgH^{[MOG]}$ B cells were co-cultured with CellTrace Violet-labeled 1C6 T cells and
723 pulsed, or not, with the indicated concentrations of $MOG_{[35-55]}$. Gate frequencies
724 indicate the percentage of cells undergoing at least one cell division.
725 Representative of triplicate cultures.
726
727 **Supplemental Figure 2. A.** Splenic immature, mature and CS B cells were
728 assessed from the same mice as in **Figure 2B**. **B.** MHC class II ($I\text{-}Ag^7$) expression
729 was assessed from CNS B cells at endpoint from $MOG_{[35-55]}$-immunized NOD (n=5)
730 or $IgH^{[MOG]}$ (n=5) mice. **C.** Germinal center B cells ($GL\text{-}7^+Fas^+$) were assessed from
731 the spleens and CNS of $MOG_{[35-55]}$-immunized NOD (n=5) or $IgH^{[MOG]}$ (n=5) mice.
732 *, $p<0.05$; ***, $p<0.001$, n.s., not significant.
733
734 **Supplemental Figure 3.** Dendritic cells ($CD11c^+$), astrocytes ($GFAP^+$), resting
735 microglia ($CD45^{dim}CD11b^{dim}$) and activated microglia ($CD45^{hi}CD11b^{hi}$) were
736 assessed for expression of p19 and p40 from the CNS of $MOG_{[35-55]}$-immunized
737 WT (n=5) or $IgH^{[MOG]}$ (n=5) mice. DCs, microglia; n=5 each group; astrocytes, n=10
738 each group.
739
740 **Supplemental Figure 4. A.** Expression of Bcl6 was assessed from WT or $IgH^{[MOG]}$
741 $PD\text{-}1^+CXCR5^-$ CNS-infiltrating T cells versus *in vitro* generated 1C6 Tfh or Th0. **B.**
742 Expression of Bcl6 was assessed from CNS-infiltrating $CD4^+$ T cells taken from

743 immunized NOD (n=6) and IgH[MOG] (n=6) mice, and expression between PD-1$^-$

744 and PD-1$^+$ CD4$^+$ subpopulations was compared.

745

746 **References**

747

748 1. Kingwell, E. *et al.* Incidence and prevalence of multiple sclerosis in Europe:
749 a systematic review. *BMC Neurol* **13,** 128 (2013).
750 2. Larochelle, C., Uphaus, T., Prat, A. & Zipp, F. Secondary Progression in
751 Multiple Sclerosis: Neuronal Exhaustion or Distinct Pathology? *Trends in*
752 *Neurosciences* **39,** 325–339 (2016).
753 3. Thompson, A. Overview of primary progressive multiple sclerosis (PPMS):
754 similarities and differences from other forms of MS, diagnostic criteria, pros
755 and cons of progressive diagnosis. *Mult. Scler.* **10 Suppl 1,** S2–7 (2004).
756 4. Baranzini, S. E. *et al.* B cell repertoire diversity and clonal expansion in
757 multiple sclerosis brain lesions. *J. Immunol.* **163,** 5133–5144 (1999).
758 5. Owens, G. P. *et al.* Restricted use of VH4 germline segments in an acute
759 multiple sclerosis brain. *Ann. Neurol.* **43,** 236–243 (1998).
760 6. Owens, G. P. *et al.* Single-cell repertoire analysis demonstrates that clonal
761 expansion is a prominent feature of the B cell response in multiple sclerosis
762 cerebrospinal fluid. *J. Immunol.* **171,** 2725–2733 (2003).
763 7. Magliozzi, R. *et al.* Meningeal B-cell follicles in secondary progressive
764 multiple sclerosis associate with early onset of disease and severe cortical
765 pathology. *Brain* **130,** 1089–1104 (2007).
766 8. Uccelli, A., Aloisi, F. & Pistoia, V. Unveiling the enigma of the CNS as a B-
767 cell fostering environment. *Trends Immunol.* **26,** 254–259 (2005).
768 9. Genain, C. P., Cannella, B., Hauser, S. L. & Raine, C. S. Identification of
769 autoantibodies associated with myelin damage in multiple sclerosis. **5,**
770 170–175 (1999).
771 10. Hauser, S. L. *et al.* B-cell depletion with rituximab in relapsing-remitting
772 multiple sclerosis. *N. Engl. J. Med.* **358,** 676–688 (2008).
773 11. Kappos, L. *et al.* Ocrelizumab in relapsing-remitting multiple sclerosis: a
774 phase 2, randomised, placebo-controlled, multicentre trial. *Lancet* **378,**
775 1779–1787 (2011).
776 12. Hauser, S. L. *et al.* Ofatumumab versus Teriflunomide in Multiple Sclerosis.
777 *N. Engl. J. Med.* **383,** 546–557 (2020).
778 13. Montalban, X. *et al.* Ocrelizumab versus Placebo in Primary Progressive
779 Multiple Sclerosis. *N. Engl. J. Med.* (2016). doi:10.1056/NEJMoa1606468
780 14. Lehmann-Horn, K., Kronsbein, H. C. & Weber, M. S. Targeting B cells in
781 the treatment of multiple sclerosis: recent advances and remaining
782 challenges. **6,** 161–173 (2013).

783 15. Rangachari, M. & Kuchroo, V. K. Using EAE to better understand principles
784 of immune function and autoimmune pathology. *J. Autoimmun.* **45,** 31–39
785 (2013).
786 16. Litzenburger, T. *et al.* B lymphocytes producing demyelinating
787 autoantibodies: development and function in gene-targeted transgenic
788 mice. *J. Exp. Med.* **188,** 169–180 (1998).
789 17. Krishnamoorthy, G., Lassmann, H., Wekerle, H. & Holz, A. Spontaneous
790 opticospinal encephalomyelitis in a double-transgenic mouse model of
791 autoimmune T cell/B cell cooperation. **116,** 2385–2392 (2006).
792 18. Pöllinger, B. *et al.* Spontaneous relapsing-remitting EAE in the SJL/J
793 mouse: MOG-reactive transgenic T cells recruit endogenous MOG-specific
794 B cells. *J. Exp. Med.* **206,** 1303–1316 (2009).
795 19. Dang, A. K., Jain, R. W., Craig, H. C. & Kerfoot, S. M. B cell recognition of
796 myelin oligodendrocyte glycoprotein autoantigen depends on immunization
797 with protein rather than short peptide, while B cell invasion of the CNS in
798 autoimmunity does not. *J. Neuroimmunol.* **278,** 73–84 (2015).
799 20. Zhong, X. *et al.* Reciprocal generation of Th1/Th17 and T(reg) cells by B1
800 and B2 B cells. *Eur. J. Immunol.* **37,** 2400–2404 (2007).
801 21. Wang, Y. & Rothstein, T. L. Induction of Th17 cell differentiation by B-1
802 cells. *Front Immunol* **3,** 281 (2012).
803 22. Barbosa, R. R. *et al.* Primary B-cell deficiencies reveal a link between
804 human IL-17-producing CD4 T-cell homeostasis and B-cell differentiation.
805 *PLoS ONE* **6,** e22848 (2011).
806 23. Bar-Or, A. *et al.* Abnormal B-cell cytokine responses a trigger of T-cell-
807 mediated disease in MS? *Ann. Neurol.* **67,** 452–461 (2010).
808 24. van de Veerdonk, F. L. *et al.* The anti-CD20 antibody rituximab reduces the
809 Th17 cell response. *Arthritis Rheum* **63,** 1507–1516 (2011).
810 25. Encinas, J. A. *et al.* QTL influencing autoimmune diabetes and
811 encephalomyelitis map to a 0.15-cM region containing Il2. *Nat. Genet.* **21,**
812 158–160 (1999).
813 26. Rao, D. A. *et al.* Pathologically expanded peripheral T helper cell subset
814 drives B cells in rheumatoid arthritis. *Nature* **542,** 110–114 (2017).
815 27. Mayo, L. *et al.* IL-10-dependent Tr1 cells attenuate astrocyte activation and
816 ameliorate chronic central nervous system inflammation. *Brain* **139,** 1939–
817 1957 (2016).
818 28. Farez, M. F. *et al.* Toll-like receptor 2 and poly(ADP-ribose) polymerase 1
819 promote central nervous system neuroinflammation in progressive EAE.
820 **10,** 958–964 (2009).
821 29. Baker, D. *et al.* Autoimmune encephalomyelitis in NOD mice is not initially
822 a progressive multiple sclerosis model. *Ann Clin Transl Neurol* **6,** 1362–
823 1372 (2019).
824 30. Legroux, L. & Arbour, N. Multiple Sclerosis and T Lymphocytes: An
825 Entangled Story. *J Neuroimmune Pharmacol* **10,** 528–546 (2015).
826 31. Anderson, A. C. *et al.* A transgenic model of central nervous system
827 autoimmunity mediated by CD4+ and CD8+ T and B cells. *J. Immunol.* **188,**
828 2084–2092 (2012).

829 32. Yeola, A. P. *et al.* Endogenous T Cell Receptor Rearrangement Represses
830 Aggressive Central Nervous System Autoimmunity in a TcR-Transgenic
831 Model on the Non-Obese Diabetic Background. *Front Immunol* **10,** 3115
832 (2019).
833 33. Doss, P. M. I. A. *et al.* Male sex chromosomal complement exacerbates the
834 pathogenicity of Th17 cells in a chronic model of central nervous system
835 autoimmunity. *Cell Rep* **34,** 108833 (2021).
836 34. Obermeier, B. *et al.* Matching of oligoclonal immunoglobulin transcriptomes
837 and proteomes of cerebrospinal fluid in multiple sclerosis. **14,** 688–693
838 (2008).
839 35. Barr, T. A. *et al.* B cell depletion therapy ameliorates autoimmune disease
840 through ablation of IL-6-producing B cells. *J. Exp. Med.* **209,** 1001–1010
841 (2012).
842 36. Duddy, M. *et al.* Distinct effector cytokine profiles of memory and naive
843 human B cell subsets and implication in multiple sclerosis. *J. Immunol.* **178,**
844 6092–6099 (2007).
845 37. Li, R. *et al.* Proinflammatory GM-CSF-producing B cells in multiple
846 sclerosis and B cell depletion therapy. *Sci Transl Med* **7,** 310ra166 (2015).
847 38. Domingues, H. S., Mues, M., Lassmann, H., Wekerle, H. &
848 Krishnamoorthy, G. Functional and pathogenic differences of Th1 and
849 Th17 cells in experimental autoimmune encephalomyelitis. *PLoS ONE* **5,**
850 e15531 (2010).
851 39. Howell, O. W. *et al.* Meningeal inflammation is widespread and linked to
852 cortical pathology in multiple sclerosis. *Brain* **134,** 2755–2771 (2011).
853 40. deLuca, L. E. S. *et al.* Substrain differences reveal novel disease-modifying
854 gene candidates that alter the clinical course of a rodent model of multiple
855 sclerosis. *J. Immunol.* **184,** 3174–3185 (2010).
856 41. Pikor, N. B. *et al.* Integration of Th17- and Lymphotoxin-Derived Signals
857 Initiates Meningeal-Resident Stromal Cell Remodeling to Propagate
858 Neuroinflammation. *Immunity* **43,** 1160–1173 (2015).
859 42. McGeachy, M. J. *et al.* The interleukin 23 receptor is essential for the
860 terminal differentiation of interleukin 17-producing effector T helper cells in
861 vivo. *Nat. Immunol.* **10,** 314–324 (2009).
862 43. Haines, C. J. *et al.* Autoimmune memory T helper 17 cell function and
863 expansion are dependent on interleukin-23. *Cell Rep* **3,** 1378–1388 (2013).
864 44. Ramgolam, V. S. *et al.* B cells as a therapeutic target for IFN-β in
865 relapsing-remitting multiple sclerosis. *J. Immunol.* **186,** 4518–4526 (2011).
866 45. Langrish, C. L. *et al.* IL-12 and IL-23: master regulators of innate and
867 adaptive immunity. *Immunol. Rev.* **202,** 96–105 (2004).
868 46. Nitsch, L. *et al.* Astrocyte-specific expression of interleukin 23 leads to an
869 aggravated phenotype and enhanced inflammatory response with B cell
870 accumulation in the EAE model. *J Neuroinflammation* **18,** 101–16 (2021).
871 47. Chen, Y. *et al.* Anti-IL-23 therapy inhibits multiple inflammatory pathways
872 and ameliorates autoimmune encephalomyelitis. *J. Clin. Invest.* **116,** 1317–
873 1326 (2006).

874 48. Quinn, J. L., Kumar, G., Agasing, A., Ko, R. M. & Axtell, R. C. Role of TFH
875 Cells in Promoting T Helper 17-Induced Neuroinflammation. *Front Immunol*
876 **9,** 382 (2018).
877 49. Zhang, F. *et al.* Defining inflammatory cell states in rheumatoid arthritis
878 joint synovial tissues by integrating single-cell transcriptomics and mass
879 cytometry. *Nat. Immunol.* **20,** 928–942 (2019).
880 50. Johnston, R. J. *et al.* Bcl6 and Blimp-1 are reciprocal and antagonistic
881 regulators of T follicular helper cell differentiation. *Science* **325,** 1006–1010
882 (2009).
883 51. Bocharnikov, A. V. *et al.* PD-1hiCXCR5- T peripheral helper cells promote
884 B cell responses in lupus via MAF and IL-21. *JCI Insight* **4,** (2019).
885 52. Schröder, J. B. *et al.* Immune Cell Activation in the Cerebrospinal Fluid of
886 Patients With Parkinson's Disease. *Front Neurol* **9,** 1081 (2018).
887 53. Field, J. *et al.* A polymorphism in the HLA-DPB1 gene is associated with
888 susceptibility to multiple sclerosis. *PLoS ONE* **5,** e13454 (2010).
889 54. Noronha, A., Toscas, A. & Jensen, M. A. Interferon beta decreases T cell
890 activation and interferon gamma production in multiple sclerosis. *J.*
891 *Neuroimmunol.* **46,** 145–153 (1993).
892 55. Duda, P. W., Schmied, M. C., Cook, S. L., Krieger, J. I. & Hafler, D. A.
893 Glatiramer acetate (Copaxone) induces degenerate, Th2-polarized immune
894 responses in patients with multiple sclerosis. *J. Clin. Invest.* **105,** 967–976
895 (2000).
896 56. Stüve, O. *et al.* Altered CD4+/CD8+ T-cell ratios in cerebrospinal fluid of
897 natalizumab-treated patients with multiple sclerosis. *Arch. Neurol.* **63,**
898 1383–1387 (2006).
899 57. Myhr, K.-M., Torkildsen, Ø., Lossius, A., Bø, L. & Holmøy, T. B cell
900 depletion in the treatment of multiple sclerosis. *Expert Opin Biol Ther* **19,**
901 261–271 (2019).
902 58. Vanderlugt, C. L. & Miller, S. D. Epitope spreading in immune-mediated
903 diseases: implications for immunotherapy. **2,** 85–95 (2002).
904 59. Crotty, S. A brief history of T cell help to B cells. *Nat. Rev. Immunol.* **15,**
905 185–189 (2015).
906 60. Mitsdoerffer, M. *et al.* Proinflammatory T helper type 17 cells are effective
907 B-cell helpers. *Proc. Natl. Acad. Sci. U.S.A.* **107,** 14292–14297 (2010).
908 61. Hartlehnert, M. *et al.* Bcl6 controls meningeal Th17-B cell interaction in
909 murine neuroinflammation. *Proc. Natl. Acad. Sci. U.S.A.* **118,** (2021).
910 62. Lee, Y. *et al.* IL-21R signaling is critical for induction of spontaneous
911 experimental autoimmune encephalomyelitis. *J. Clin. Invest.* **125,** 4011–
912 4020 (2015).
913 63. Xiao, S. *et al.* Checkpoint Receptor TIGIT Expressed on Tim-1+ B Cells
914 Regulates Tissue Inflammation. *Cell Rep* **32,** 107892 (2020).
915 64. Liu, Z. *et al.* Increased circulating PD-1hiCXCR5- peripheral T helper cells
916 are associated with disease activity of ANCA-associated vasculitis. *Clin.*
917 *Exp. Immunol.* **207,** 287–296 (2022).

65. Boivin, N., Baillargeon, J., Doss, P. M. I. A., Roy, A.-P. & Rangachari, M. Interferon-β suppresses murine Th1 cell function in the absence of antigen-presenting cells. *PLoS ONE* **10,** e0124802 (2015).
66. Rojas, O. L. *et al.* Recirculating Intestinal IgA-Producing Cells Regulate Neuroinflammation via IL-10. *Cell* **176,** 610–624.e18 (2019).
67. Gao, X., Wang, H., Chen, Z., Zhou, P. & Yu, D. An optimized method to differentiate mouse follicular helper T cells in vitro. *Cell. Mol. Immunol.* **17,** 779–781 (2020).

Figure 1.

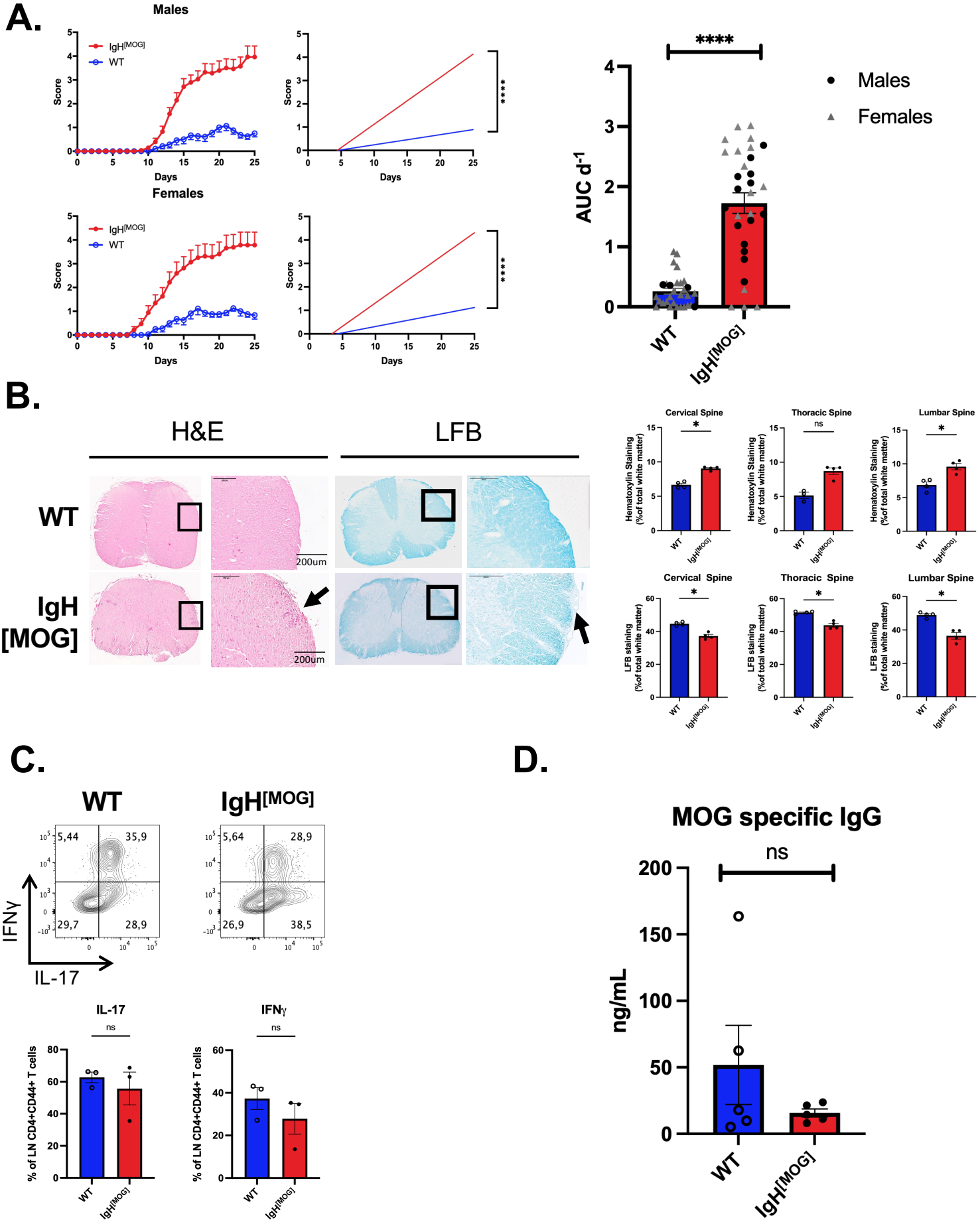
A.
Males
IgH[MOG]
WT
Score
Days
****
Females
AUC d-1
Males
Females
B.
H&E
LFB
WT
IgH [MOG]
200um
Cervical Spine
Thoracic Spine
Lumbar Spine
Hematoxylin Staining (%of total white matter)
LFB staining (%of total white matter)
ns
C.
WT
IgH[MOG]
5,44
35,9
29,7
28,9
5,64
28,9
26,9
38,5
IFNγ
IL-17
% of LN CD4+CD44+ T cells
D.
MOG specific IgG
ng/mL

Figure 2.

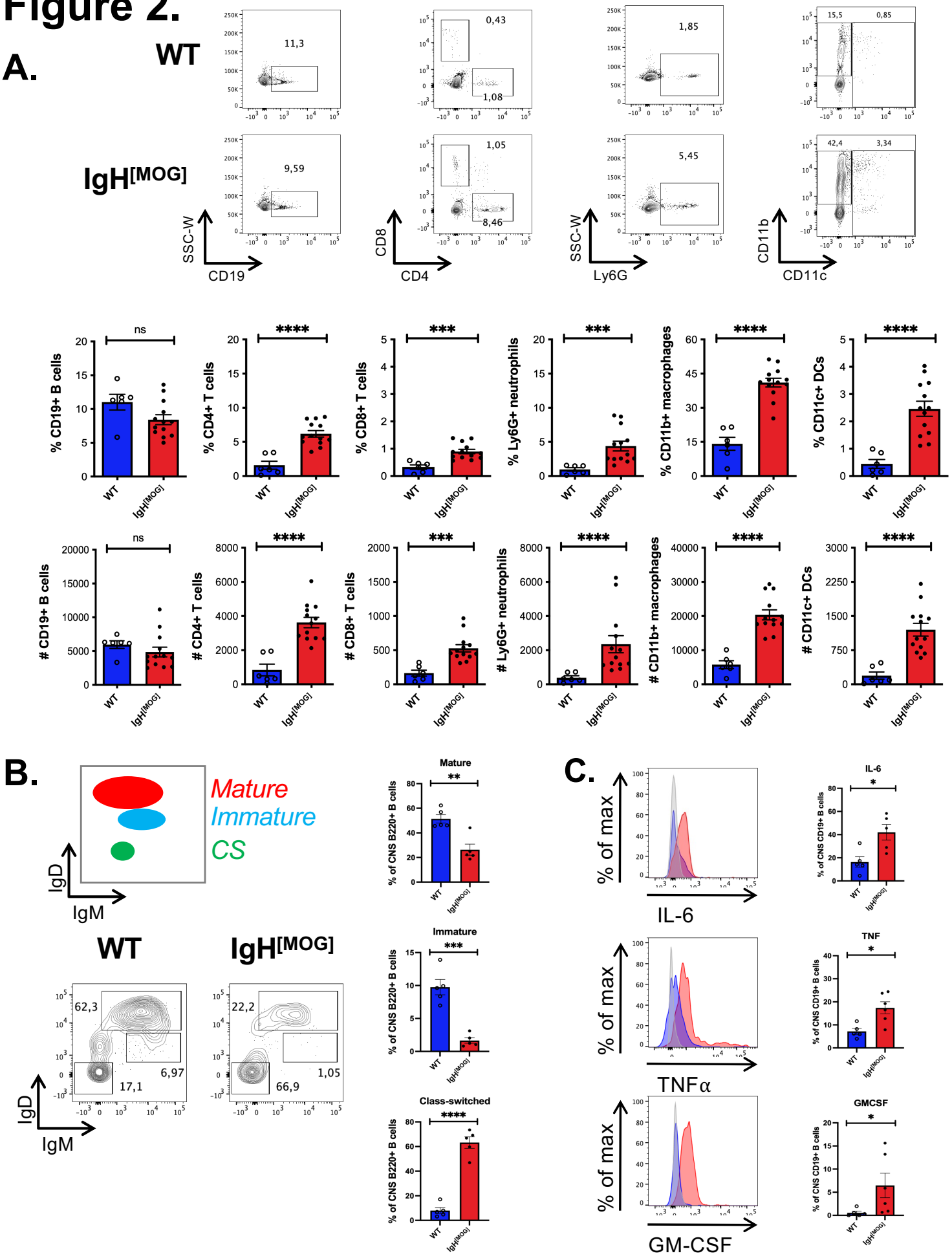
A.
WT
IgH[MOG]
11,3
9,59
0,43
1,08
1,05
8,46
1,85
5,45
15,5
0,85
42,4
3,34
SSC-W
CD19
CD8
CD4
SSC-W
Ly6G
CD11b
CD11c
% CD19+ B cells
% CD4+ T cells
% CD8+ T cells
% Ly6G+ neutrophils
% CD11b+ macrophages
% CD11c+ DCs
# CD19+ B cells
# CD4+ T cells
# CD8+ T cells
# Ly6G+ neutrophils
# CD11b+ macrophages
# CD11c+ DCs
ns
****
***
WT
IgH[MOG]
B.
Mature
Immature
CS
IgD
IgM
WT
IgH[MOG]
62,3
17,1
6,97
22,2
66,9
1,05
Mature
Immature
Class-switched
% of CNS B220+ B cells
**
***
****
C.
% of max
IL-6
TNFα
GM-CSF
% of CNS CD19+ B cells
*

Figure 3.

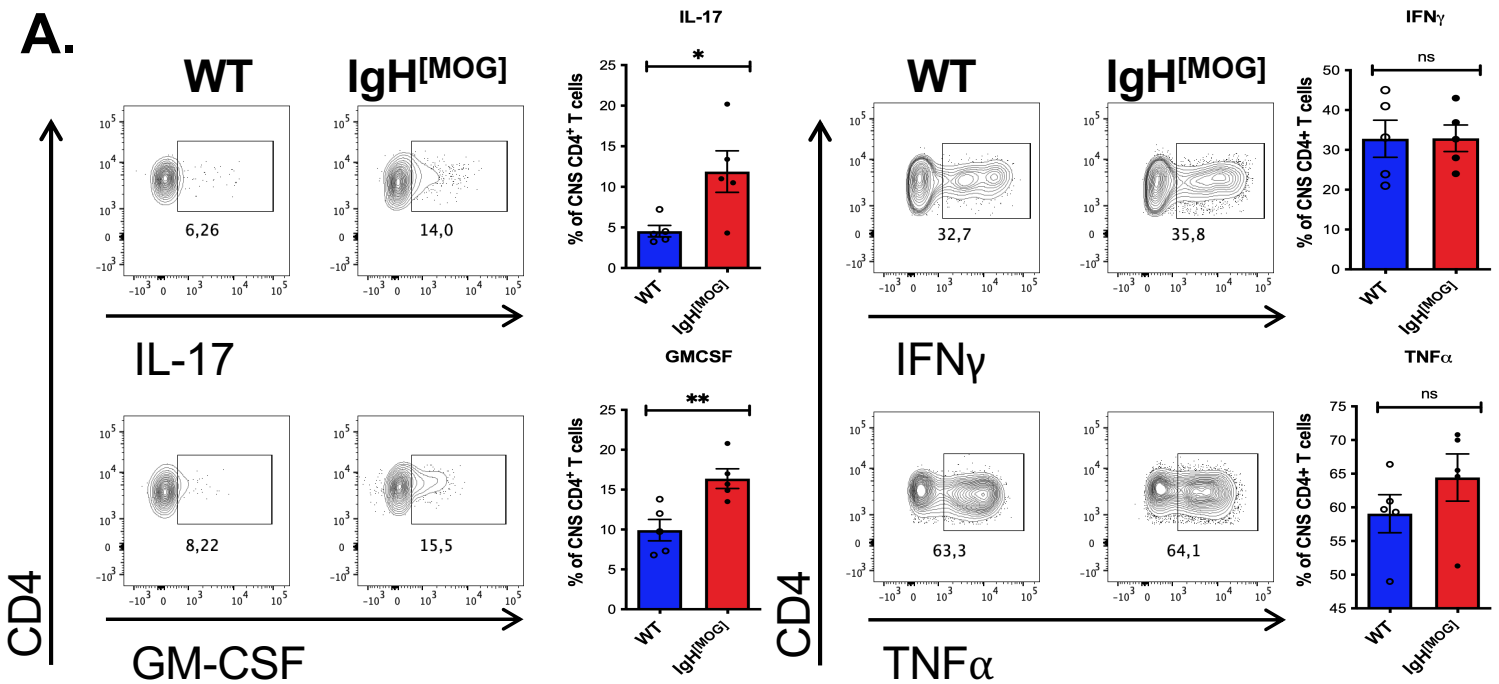
A.
WT
IgH[MOG]
6,26
14,0
IL-17
8,22
15,5
GM-CSF
CD4
IL-17
GMCSF
% of CNS CD4+ T cells
*
**
WT
IgH[MOG]
32,7
35,8
IFNγ
63,3
64,1
TNFα
CD4
IFNγ
TNFα
ns
ns

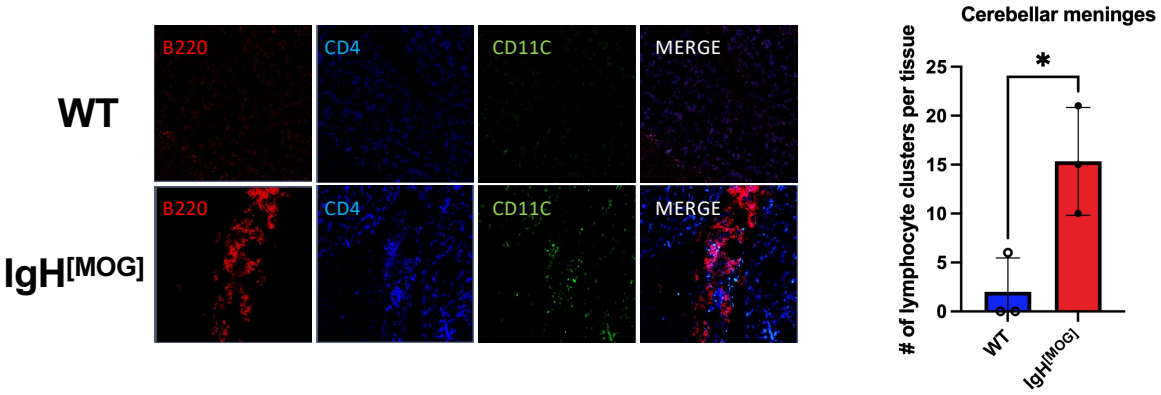
B.
WT
IgH[MOG]
B220
CD4
CD11C
MERGE
Cerebellar meninges
# of lymphocyte clusters per tissue
*
WT
IgH[MOG]

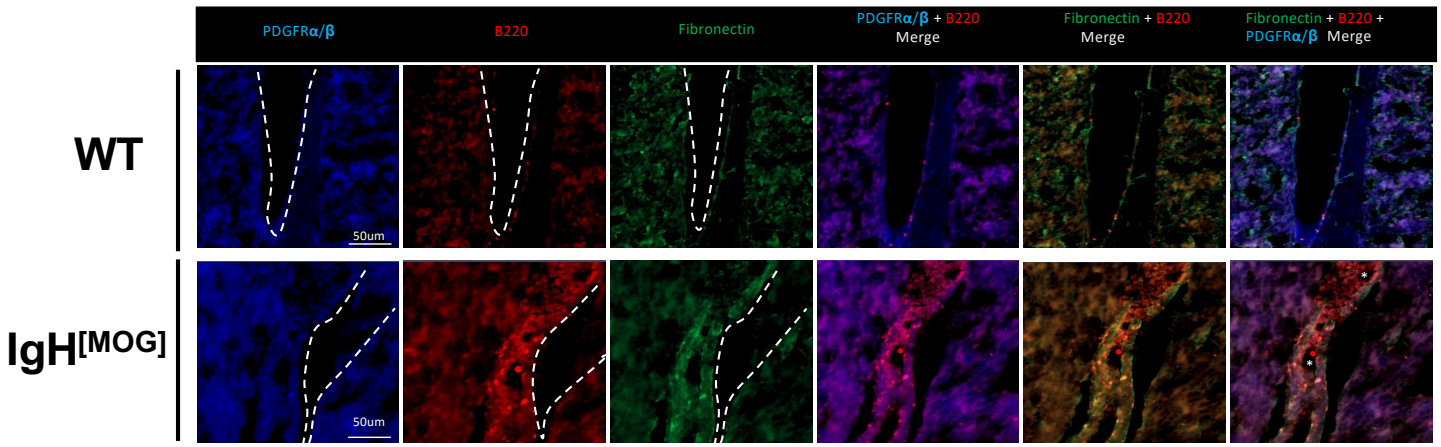
C.
PDGFRα/β
B220
Fibronectin
PDGFRα/β + B220 Merge
Fibronectin + B220 Merge
Fibronectin + B220 + PDGFRα/β Merge
WT
IgH[MOG]
50um
50um

Figure 4.

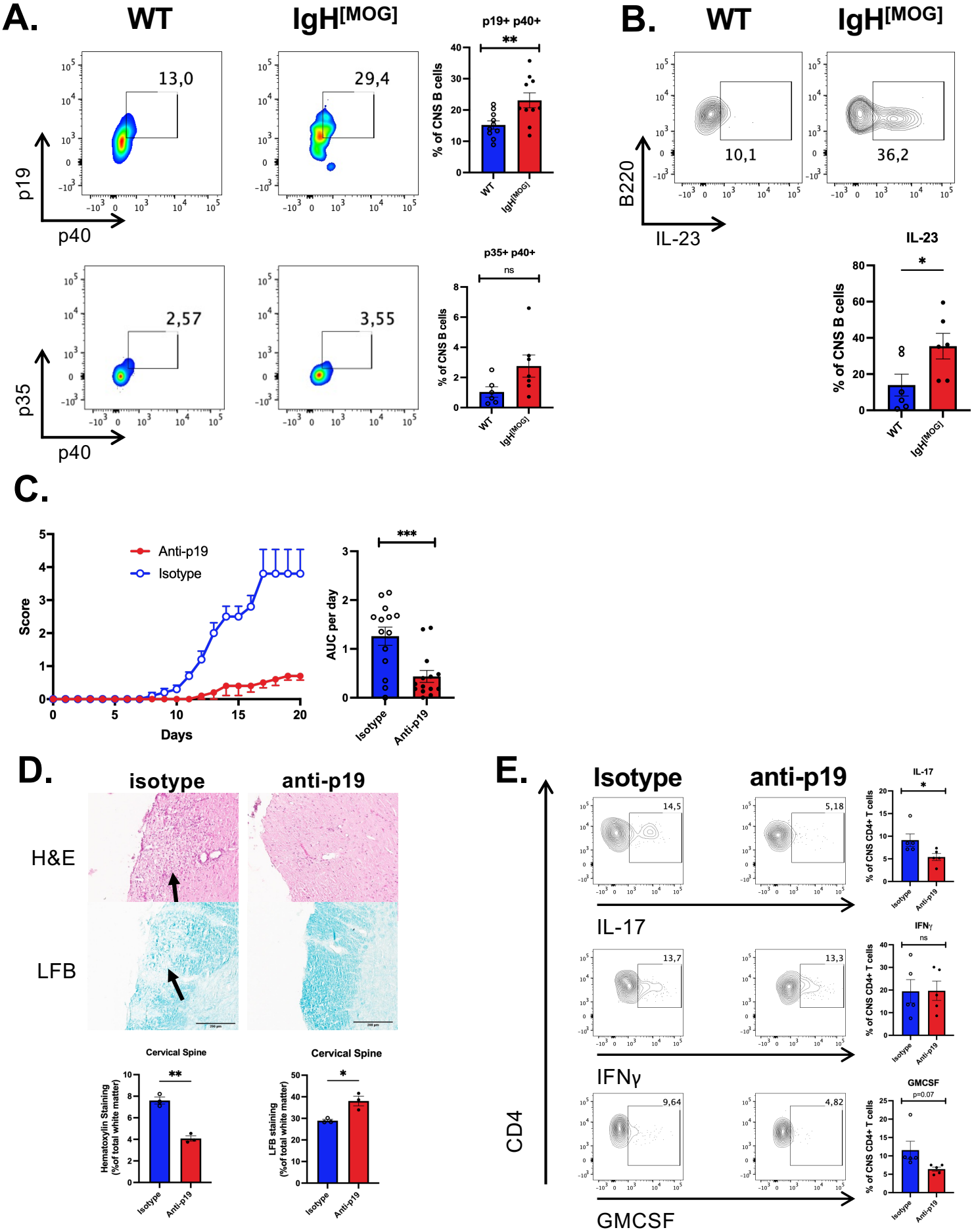
A.
WT
IgH[MOG]
13,0
29,4
p19
p40
p19+ p40+
**
% of CNS B cells
WT
IgH[MOG]
2,57
3,55
p35
p40
p35+ p40+
ns
B.
WT
IgH[MOG]
10,1
36,2
B220
IL-23
IL-23
*
C.
Anti-p19
Isotype
Score
Days
***
AUC per day
Isotype
Anti-p19
D.
isotype
anti-p19
H&E
LFB
Cervical Spine
Hematoxylin Staining (%of total white matter)
**
Cervical Spine
LFB staining (%of total white matter)
*
E.
Isotype
anti-p19
14,5
5,18
IL-17
IL-17
*
% of CNS CD4+ T cells
13,7
13,3
IFNγ
IFNγ
ns
9,64
4,82
GMCSF
GMCSF
p=0.07
CD4

Figure 5.

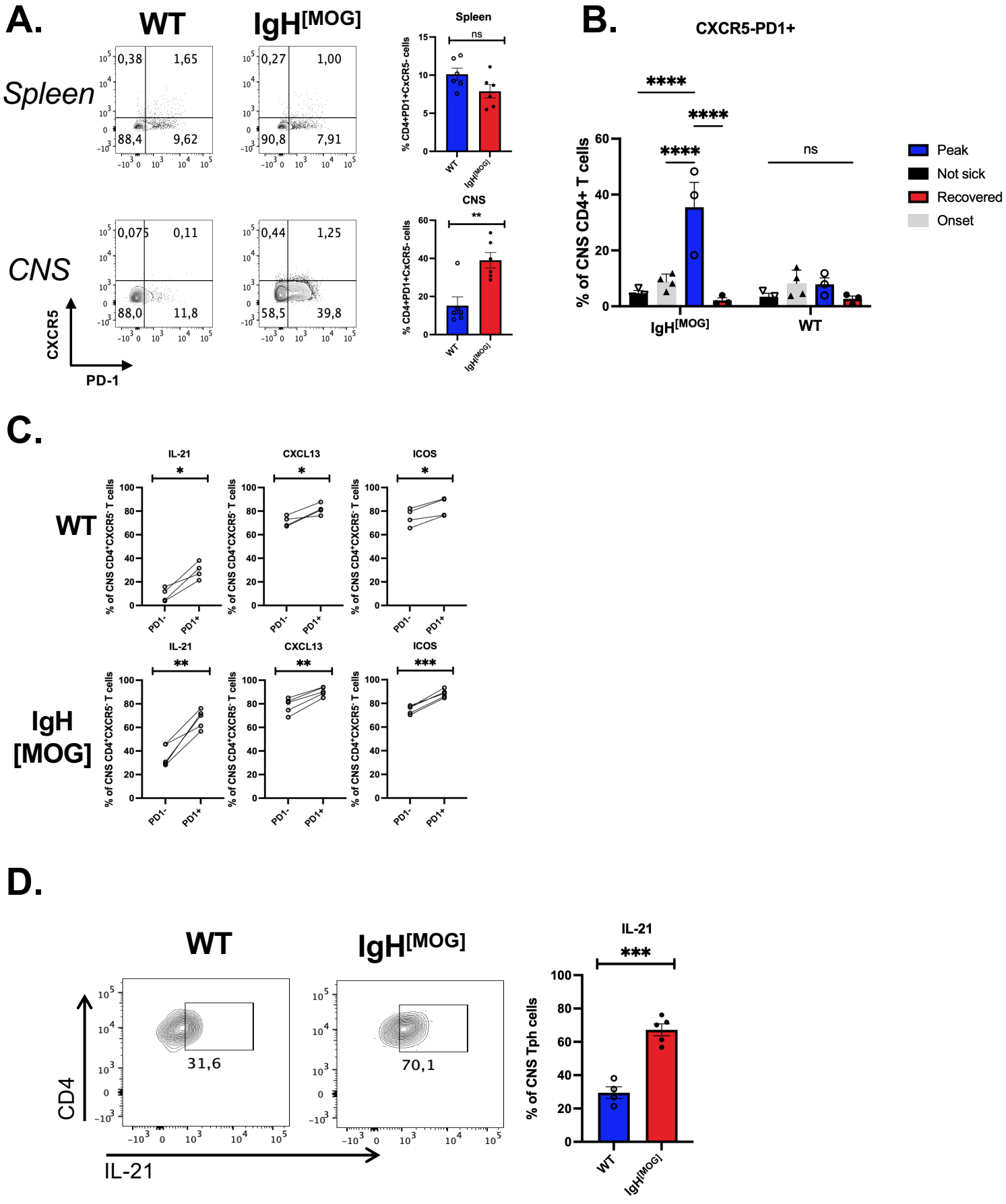
A.
WT
IgH[MOG]
Spleen
CNS
0,38
1,65
88,4
9,62
0,27
1,00
90,8
7,91
0,075
0,11
88,0
11,8
0,44
1,25
58,5
39,8
CXCR5
PD-1
Spleen
ns
% CD4+PD1+CxCR5- cells
CNS
**
% CD4+PD1+CxCR5- cells
WT
IgH[MOG]
B.
CXCR5-PD1+
****
****
****
ns
% of CNS CD4+ T cells
IgH[MOG]
WT
Peak
Not sick
Recovered
Onset
C.
WT
IgH [MOG]
IL-21
CXCL13
ICOS
% of CNS CD4+CXCR5- T cells
PD1-
PD1+
D.
WT
IgH[MOG]
31,6
70,1
CD4
IL-21
IL-21
***
% of CNS Tph cells
WT
IgH[MOG]

Figure 6.

A.

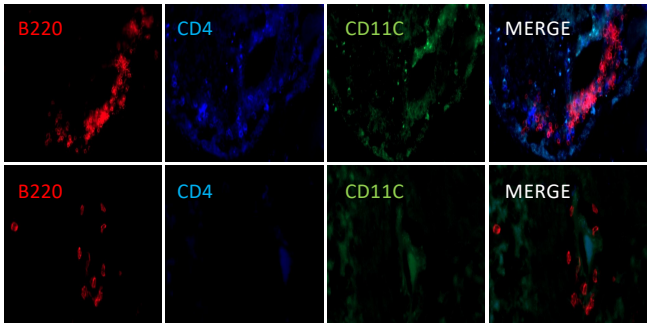

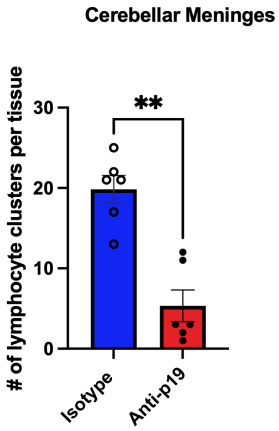

B.

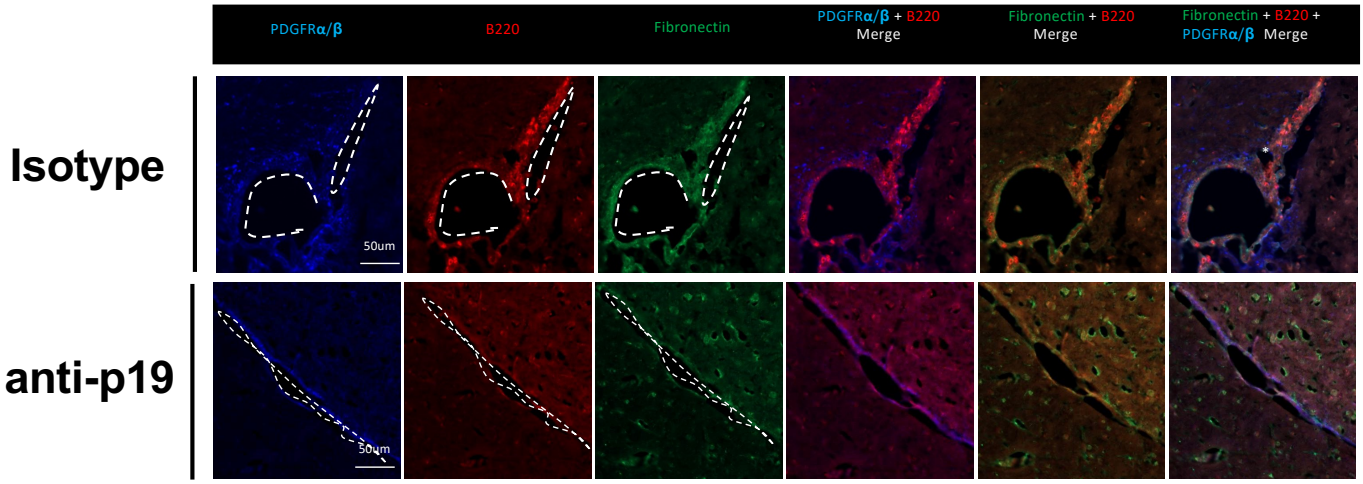

C.

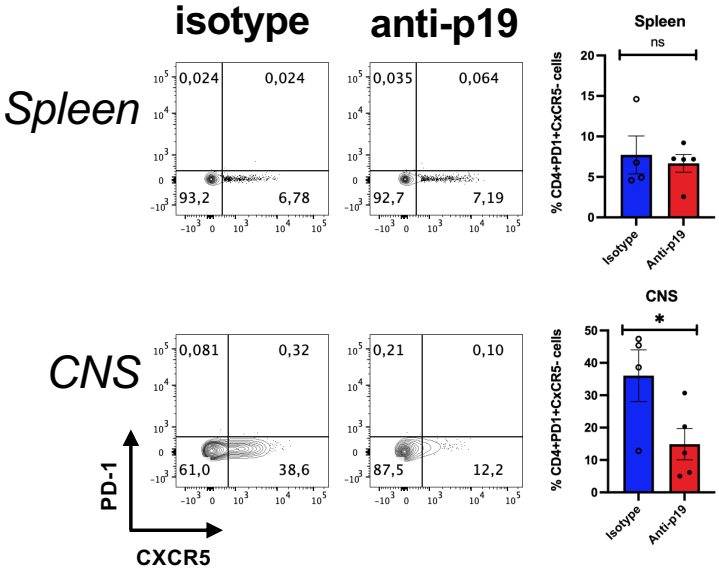
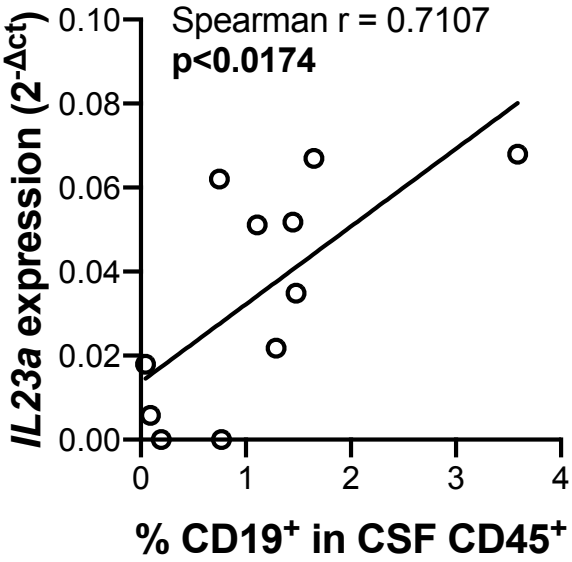
D.